Published in final edited form as:

Clin Cancer Res. 2020 July 15; 26(14): 3608–3615. doi:10.1158/1078-0432.CCR-20-0268.

Theranostic targeting of CUB domain containing protein 1 (CDCP1) in pancreatic cancer

Anna Moroz[1,2], **Yung-hua Wang**[1], **Jeremy M. Sharib**[3], **Junnian Wei**[1], **Ning Zhao**[1], **Yangjie Huang**[1], **Zhuo Chen**[1], **Alex J. Martinko**[4], **Jie Zhuo**[4], **Shion A. Lim**[4], **Lydia Zhang**[4], **Youngho Seo**[1], **Sean D. Carlin**[5], **Kevin K. Leung**[4], **Eric A. Collisson**[6,7], **Kimberly S. Kirkwood**[3,7], **James A. Wells**[4,7], **Michael J. Evans**[1,4,7]

[1]Department of Radiology and Biomedical Imaging, University of California San Francisco, 505 Parnassus Ave, San Francisco CA 94143

[2]Skolkovo Institute of Science and Technology, Skolkovo Innovation Center, 3 Nobel Street, Moscow 143026, Russia

[3]Department of Surgery, University of California San Francisco, 505 Parnassus Ave, San Francisco CA 94143

[4]Department of Pharmaceutical Chemistry, University of California San Francisco, 505 Parnassus Ave, San Francisco CA 94143

[5]Department of Radiology, University of Pennsylvania, 3400 Spruce Street, 1 Silverstein Philadelphia, PA 19104

[6]Department of Medicine, University of California San Francisco, 505 Parnassus Ave, San Francisco CA 94143

[7]Helen Diller Family Comprehensive Cancer Center, University of California San Francisco, 505 Parnassus Ave, San Francisco CA 94143

Abstract

Purpose: The recent emergence of radioligand therapies for cancer treatment has increased enthusiasm for developing new theranostic strategies coupling both imaging and cytotoxicity in the same entity. In this study, we evaluated if CUB domain containing protein 1 (CDCP1), a single pass transmembrane protein highly overexpressed in diverse human cancers, might be a target for cancer theranostics.

Corresponding author: Michael J. Evans, PhD, Tel: 415-514-1292, Michael.evans@ucsf.edu.

Author Contributions:

Conception and design: A. Moroz, J.A. Wells, M.J. Evans

Acquisition of data: A. Moroz, J. Sharib, A. Martinko, Y. Wang, J. Wei, N. Zhao, Y. Huang, Z. Chen, L. Zhang, S.A. Lim, J. Zhuo, S.D. Carlin, K. Kirkwood

Analysis and interpretation of data: A. Moroz, J. Sharib, J. Sharib, Y. Huang, Y. Seo, K.K. Leung, E.A. Collisson, K. Kirkwood, J.A. Wells, M.J. Evans

Writing, review, and/or revision of the manuscript: A. Moroz, J. Sharib, Y. Seo, K.K. Leung, E.A. Collisson, K. Kirkwood, J.A. Wells, M.J. Evans

Disclosure of potential conflicts of interest: J.A. Wells receives research support from Celgene Corporation. A patent encompassing the structure and uses of 4A06 has been filed by the Regents of the University of California.

Experimental Design: The ectodomain of CDCP1 was targeted using radiolabeled forms of 4A06, a potent and specific recombinant human antibody that we developed. Imaging and antitumor assessment studies were performed in animal models of pancreatic cancer, including two PDX models we developed for this study. For antitumor assessment studies, the endpoints were death due to tumor volume >3000 mm^3 or ≥20% loss in body weight. Specific tracer binding or antitumor effects were assessed with an unpaired, two-tailed Student's t test and survival advantages were assessed with a log rank (Mantel Cox) test. Differences at the 95% confidence level were interpreted to be significant.

Results: ^{89}Zr-4A06 detected a broad dynamic range of full length or cleaved CDCP1 expression on seven human pancreatic cancer tumors (n = 4/tumor). Treating mice with single or fractionated doses of ^{177}Lu-4A06 significantly reduced pancreatic cancer tumor volume compared to mice receiving vehicle or unlabeled 4A06 (n = 8, P<0.01). A single dose of ^{225}Ac-4A06 also inhibited tumor growth, although the effect was less profound compared to ^{177}Lu-4A06 (n = 8, P<0.01). A significant survival advantage was imparted by ^{225}Ac-4A06 (HR = 2.56, P <0.05).

Conclusions: These data establish that CDCP1 can be exploited for theranostics, a finding with widespread implications given its breadth of overexpression in cancer.

Introduction:

The recent clinical successes of radioligand therapies (e.g. Lutathera, Azedra) have rejuvenated enthusiasm for implementing theranostic platforms to treat cancer (1). Realizing the clinical potential of radioligand therapy requires (in part) identifying new protein targets that satisfy the prerequisites of this approach, which include high, and preferably tumor specific target expression, and accessibility of the target to a potent and specific ligand. Ideally, the target would also be overexpressed in many tumor types.

We appreciated that the protein CUB domain containing protein 1 (CDCP1, also known as CD318 or Transmembrane and associated with Src kinase (TRASK)) appeared to satisfy many of these prerequisites. CDCP1 is a single pass, glycosylated transmembrane protein expressed on the cell surface, which renders it very accessible to exogenous ligands for imaging or treatment applications (2, 3). Moreover, CDCP1 can be highly overexpressed in human tumor tissue from cancers as diverse as prostate, breast, lung, ovarian, pancreatic, and kidney, and overexpression associates with more aggressive forms of these cancers (4–10). Indeed, we previously quantified CDCP1 receptor density and found it to be commensurate (~10^6 receptors/cell) with values reported for other highly abundant theranostic targets (e.g. SSTR2, PSMA, HER2, see Supplemental Table 1)(11). Mechanism studies sensibly rationalize the remarkable breadth of cancer overexpression, as CDCP1 transcription is regulated by numerous prominent oncogenic signaling pathways. Examples include Ras/Raf/MEK/ERK signaling, HIF2α transcriptional activity driven by hypoxia or VHL deletion, and TGFβ/Smad2/3 signaling(9, 12, 13). Lastly, CDCP1 mRNA levels are consistently higher in cancer compared to the respective normal tissue from which it arises, and homozygous germline CDCP1 knockout mice develop without any measurable phenotype and have a normal lifespan.(14)

Ongoing work is also revealing that CDCP1 may contribute to cancer pathophysiology. For instance, full length, phosphorylated CDCP1 augments metastatic potential by binding and activating PKCδ, and/or by inhibiting long chain fatty acid coA ligase 3(15, 16). CDCP1 also physically interacts with important cancer signaling molecules (e.g. EGFR and integrins) to activate intracellular oncogenic signaling(17, 18). Moreover, genetic ablation of CDCP1 inhibits anchorage independent growth and metastasis(19, 20). Expression-driven phenotypes align well with the clinical data showing poorer outcomes for tumors with CDCP1 overexpression. Collectively, these observations support the rationale for targeting CDCP1 therapeutically.

We report herein the first data establishing that CDCP1 can be targeted with a radiolabeled antibody for cancer theranostics. We performed these studies using 4A06, a potent and specific recombinant human antibody we developed against the ectodomain of CDCP1(11). Proof of concept was established using human cancer cell lines and patient derived xenografts (PDX) of pancreatic ductal adenocarcinoma, as CDCP1 is commonly overexpressed in this malignancy(10, 21), and there is an urgent unmet clinical need to develop new therapies to treat this highly morbid disease. A broad dynamic range of tumor autonomous expression of CDCP1 was detectable in vivo with ^{89}Zr-labeled 4A06 and PET/CT. Treating tumor bearing mice with a single or fractionated dose of ^{177}Lu-labeled 4A06 profoundly suppressed tumor growth compared to mice receiving no treatment or a 10 fold molar excess of unlabeled 4A06. As the antibody receptor complex internalizes into cells, we also evaluated the antitumor effects of single dose ^{225}Ac-4A06. Interestingly, tumor progression was delayed by ^{225}Ac-4A06, but the antitumor effects were milder compared to our findings with ^{177}Lu-4A06. In summary, these data show for the first time that CDCP1 can be targeted with radioligands for theranostics, findings that we expect to motivate additional studies to identify the optimal platform for fully exploiting this tumor antigen.

Materials and Methods

Primary Tumor Collection

The study protocol and design were approved by the UCSF Institutional Review Board, and all studies involving human subjects were conducted in compliance with the U.S. Common Rule. Patient recruitment and enrollment was completed through the Surgical Oncology Clinic at UCSF and patients provided written informed consent authorizing collection and use of tumor tissue and clinical data for study purposes. Pancreatic tumors were collected from the operating room at the time of surgical resection by the UCSF Biospecimen Resources Program and divided for clinical pathologic review and research purposes from the time of the biorepository creation to publication. Between 0.2–1g fresh primary tumor tissue was provided to the research coordinator in Liebowitz media with 5 ug/ul penicillin and streptomycin within 1 hour of resection and engrafted in NOD scid gamma (NSG) mice as described below within 2–4 hours.

Animal studies

All animal studies were conducted in compliance with Institutional Animal Care and Use Committee at UCSF. For tumor imaging or treatment studies, three to five-week-old intact male athymic nu/nu mice were purchased from Charles River and used for experiments after a brief period of acclimation. Mice were inoculated subcutaneously with human pancreatic cancer cells (~1.5×10^6) in the flank. The cells were injected in a 1:1 mixture (v/v) of media (DMEM/F12) and Matrigel (Corning). Xenografts were generally palpable within 14–18 days after injection.

Primary tumor specimens were engrafted as soon as possible into NSG mice on the same day as primary resection. Tissue was never frozen or dried from the time of resection to the time of engraftment. Primary engraftment was performed orthotopically into the pancreas. The primary tumor was dissected free of debris, normal pancreas, and clearly necrotic tissue. Tumor was minced into 0.5–1mm fragments in media on a petri dish, covered and set aside for implantation. Mice were anesthetized and positioned on their right flanks. Abdominal and left flank fur was clipped and the skin prepped with Betadine. A 0.5cm skin incision was made over the left flank inferior to the costal margin. The peritoneal cavity was then entered and the pancreas identified by its attachment to the spleen. The spleen was retracted out of the wound to spread the pancreas flat and incise the thin retroperitoneal layer overlying the pancreatic tissue, and a small pocket was created. Tumor fragment was then inserted into the pancreatic tissue through the retroperitoneal incision and the spleen and pancreas were carefully placed back into the peritoneal cavity. The peritoneum was closed with a running 5–0 vicryl suture and the skin closed with wound clips, which were removed within 10–14 days per institutional standards. The tumors were propagated subcutaneously prior to animal imaging studies.

Small animal PET/CT

All data, including the raw imaging files, are available upon request. Tumor-bearing mice received between ~200 μCi of ^{89}Zr-4A06 in 100 μL saline solution volume intravenously using a custom mouse tail vein catheter with a 28-gauge needle and a 100–150 mm long polyethylene microtubing. After a dedicated period of uptake time, mice were anesthetized with isoflurane and imaged on a small animal PET/CT scanner (Inveon, Siemens Healthcare, Malvern, PA). Animals were scanned for 40 minutes for PET, and the CT acquisition was performed for 10 minutes.

The co-registration between PET and CT images was obtained using the rigid transformation matrix generated prior to the imaging data acquisition since the geometry between PET and CT remained constant for each of PET/CT scans using the combined PET/CT scanner. The photon attenuation was corrected for PET reconstruction using the co-registered CT-based attenuation map to ensure the quantitative accuracy of the reconstructed PET data. Decay corrected images were analyzed using AMIDE software.

SPECT/CT: Mice received an intravenous injection of ^{177}Lu-4A06 (~300 μCi/mouse). After a dedicated uptake time, the mice were anesthetized and transferred to a small animal SPECT/CT (VECTor4CT, MILabs, Utrecht, The Netherlands) for imaging. The co-

registered CT was used for photon attenuation correction in the SPECT reconstruction. The decay corrected images were reconstructed and analyzed using AMIDE software.

Biodistribution studies: At a dedicated time after radiotracer injection, animals were euthanized by cervical dislocation. Blood was harvested via cardiac puncture. Tissues were removed, weighed and counted on a Hidex automatic gamma counter for accumulation activity. The mass of the injected radiotracer was measured and used to determine the total number of CPM by comparison with a standard of known activity. The data were background- and decay-corrected and expressed as the percentage of the injected dose/ weight of the biospecimen in grams (%ID/g).

Digital autoradiography: Post mortem, tumors were harvested, transferred to sample boats, and immersed in Tissue–Plus OCT compound (Scigen, Gardena, CA). The tissues were snap frozen at −80° C. The tumor tissue was sectioned into10 μm slices using a microtome and mounted on glass microscope slides. The slides were loaded onto an autoradiography cassette and exposed with film for 24–72 hours at −20° C. The film was developed and read on a Typhoon 7000IP plate reader (GE Healthcare, Chicago, IL) at 25 μm pixel resolution. The slides were counterstained with H&E. A Zeiss Axioplan2 microscope was used to develop microscopic images. MetaMorph software (Molecular Devices, Sunnyvale, CA) and Photoshop CS6 software (Adobe Systems, McLean, VA) were used for montage and processing. The autoradiography and histology were analyzed using ImageJ.

Animal treatment studies: Mice bearing unilateral subcutaneous HPAC tumors received ^{177}Lu-4A06, 4A06, ^{225}Ac-4A06 or vehicle (saline) at the indicated dose via tail vein. Animals were weighed at the time of injection, and once weekly until the completion of the study. Tumor volume measurements were calculated with calipers. For treatment studies, the primary endpoints were death due to tumor volume >3000 mm^3 or ≥ 20% loss in mouse body weight.

Statistical analysis: Data were analyzed using PRISM v8.0 software (Graphpad, San Diego, USA). Binary comparisons between two treatment arms were made with an unpaired, two-tailed Student’s t-test. Differences at the 95% confidence level ($P < 0.05$) were considered to be statistically significant. Analysis of statistically significant changes in Kaplan Meier survival curves were made with a log rank test. Differences at the 95% confidence level were considered statistically significant. For treatment studies, the primary endpoints were death due to tumor volume >3000 mm^3 or ≥ 20% loss in mouse body weight. For blocking studies, sample size was prospectively estimated using an anticipated effect size of 0.5 between the tracer uptake in blocked versus unblocked tumor and type I error rate of 0.05. For treatment studies, sample size was estimated based on an expected effect size of 0.2 for tumor volume changes with a type I error rate of 0.05.

Results:

^{89}Zr-labeled 4A06 specifically detects tumor autonomous expression of CDCP1.

We identified the 4A06 antibody by conducting phage display screening against the ectodomain of recombinant human CDCP1. The antibody binds to an epitope that is contained in both the full length and cleaved forms of CDCP1. The Fab that emerged from this initial screen was converted to an IgG1 format using standard cloning techniques and expressed using the Expi293 expression system. We opted to conduct proof of concept imaging and antitumor assessment studies with the IgG1 initially as the long biological half-life of the IgG1 would ensure durable presentation of the tumor to CDCP1.

We first functionalized the 4A06 IgG1 with the chelate, desferrioxamine (DFO), for PET/CT studies by reacting commercial para-isothiocyanatobenzyl-DFO with solvent exposed ε-amino groups on lysine residues. The affinity of DFO-4A06 for the recombinant human ectodomain of CDCP1 was assessed using biolayer interferometry (BLI); the K_D of the DFO-conjugated antibody was equivalent to unmodified 4A06 (0.40 ±0.7 nM and 0.27±0.04 nM, respectively, see Supplemental Figure 1). In anticipation of future studies with Lu-177 and Ac-225 conjugates, the antibody was also coupled to the chelator 1,4,7,10-tetraazacyclododecane-1,4,7,10-tetraacetic acid (DOTA) via similar chemistry. The affinity of DOTA-4A06 was also equivalent to unlabeled 4A06 (K_D = 0.30 ± 0.05 nM, see Supplemental Figure 1).

DFO-4A06 was radiolabeled with Zr-89 as we and others have shown that the long radioactive half-life (78.41 hours) is appropriate for studying the biodistribution of molecules with long biological half-lives(22). DFO-4A06 was incubated with ^{89}Zr-oxalic acid for 120 min and purified using size exclusion chromatography. The radiochemical yield was consistently >95%, the radiochemical purity >98%, and the specific activity was consistently ~3 μCi/μg and the molar activity was ~0.45 Ci/μmol over multiple radiosyntheses.

To evaluate biodistribution over time, ^{89}Zr-4A06 was first administered to intact male nu/nu mice bearing subcutaneous HPAC tumors, a human pancreatic adenocarcinoma cell line with an endogenous *KRAS*^{G12V} mutation that we previously showed expresses 2 × 10^6 receptors/cell. Tumor uptake of the radiotracer was visually obvious on PET/CT at 12 hours post injection, and the amount of radiotracer steadily increased out to 72 hours post injection (Figure 1A). Analysis of tissue biodistribution ex vivo corroborated this trend, showing the highest radiotracer uptake in the HPAC tumors occurred at 72 hours (n = 5/time point, see Figure 1B, Supplemental Figure 2). Moreover, the radiotracer steadily cleared from blood and normal mouse tissues from 24 – 72 hours, as expected. Little uptake was observed in normal pancreas, consistent with previous data showing low CDCP1 expression in this tissue (10). Some uptake was observed in bone, which may be attributable to radiotracer catabolism (23). A separate cohort of mice (n = 5/arm) received ^{89}Zr-4A06 with 20x molar excess unlabeled 4A06. PET/CT and biodistribution studies 48 hours post injection showed that excess unlabeled 4A06 suppressed radiotracer uptake in the tumor, confirming that ^{89}Zr-4A06 accumulation in tumors is due to specific receptor binding (Figure 1C and Supplemental Figure 3). Lastly, a separate cohort of mice bearing HPAC tumors were

injected with ^{18}F-FDG, the gold standard and most widely applied radiotracer for tumor detection. ^{18}F-FDG uptake in the tumor was significantly lower than ^{89}Zr-4A06 radiotracer, and the tumor to blood ratio for ^{89}Zr-4A06 was higher than ^{18}F-FDG. Both observations suggest that ^{89}Zr-4A06 may have applications for detection of PDAC disease burden, which can be occult on ^{18}F-FDG PET (Figure 1D).

We next evaluated if ^{89}Zr-4A06 could detect CDCP1 expression in a larger panel of PDAC models (HPAF II, Capan-1, Panc10.05, Panc2.03) with varying concentrations of full length or cleaved CDCP1 (though total CDCP1 was lower than the levels found in HPAC, see Figure 2A). Antigen recognition on viable cells with 4A06 was confirmed with flow cytometry prior to conducting the imaging study (Figure 2B). Subsequently, ^{89}Zr-4A06 was administered to mice bearing subcutaneous tumor implants of one of the cell lines. Biodistribution data showed radiotracer accumulation in the tumors at 72 hours post injection above blood and muscle activities (n = 4/tumor, see Figure 2C). Although the flow cytometry data shows variable antigen expression among the cell lines, the biodistribution data shows equivalent radiotracer uptake between the tumors. Directly correlating protein expression levels on flow cytometry in vitro with %ID/g in tumors is complicated, as radiotracer uptake in tumors is a combined measure of antibody binding and receptor mediated internalization, and radiotracer catabolism over days. Tumor microenvironment factors like hypoxia can upregulate CDCP1 expression on tumor cells (9), which may also impact the relative levels of radiotracer uptake. However, we were encouraged to observe that radiotracer uptake was significantly lower in the four tumor models compared to HPAC, as predicted based on the immunoblot data (Supplemental Table 2).

While cancer cell line models are convenient, they are known to adopt or lose crucial biological features during the process of acclimation to in vitro culture conditions. On this basis, we next isolated patient derived xenografts (PDX) to determine if CDCP1 is expressed and detectable using ^{89}Zr-4A06. One PDX, termed UCPDAC-187, was established from a tissue sample acquired during surgery of a patient with moderately high risk ypT3N1 PDAC. Tumor sequencing using the UCSF 500 gene panel revealed that the PDX harbored pathogenic mutations in KRAS (G12V), TP53, and the RNA regulatory protein U2AF1 (Supplemental Table 3). The second PDX, termed UCPAsC-208, was isolated from the surgical tissue of a patient found to have adenosquamous carcinoma of the pancreas. Genomic analysis showed it to bear pathogenic or likely pathogenic mutations in KRAS (G12D), TP53, SMAD4, ARID2, KMT2D, ad CDKN2A (Supplemental Table 3). Flow cytometry of single cell suspensions with 4A06 showed that both PDXes expressed CDCP1 (Figure 3A). PET/CT and biodistribution studies showed that ^{89}Zr-4A06 detected subcutaneous implants of either PDX in nu/nu mice (n = 4/tumor, see Figure 3C). We performed autoradiography on PDX slices post mortem to understand distribution of the antibody within the tumor. The pseudocolor showed high levels of ^{89}Zr-4A06 around the periphery of the tumor that overlapped with regions of viable tissue defined on H&E (Figure 3D and Supplemental Figure 4).

Antitumor assessment studies with ^{177}Lu- or ^{225}Ac-4A06.

We next tested if PDAC tumors could be treated with a radiolabeled form of 4A06. The autoradiography data showed partial penetration of the antibody within tumors, so we opted to first test ^{177}Lu-labeled 4A06, as the β- emissions might produce crossfire effects to treat cells within the tumor to which 4A06 is not bound. DOTA-4A06 was coupled to commercial $^{177}LuCl_3$ at room temperature in aqueous buffer for 120 min. The radiotracer was purified using size exclusion chromatography. The radiochemical yield prior to purification was consistently >90% with a final purity >99%. The specific activity was calculated to be approximately 9 μCi/μg (molar activity ~ 1.35 Ci/μmol).

^{177}Lu-4A06 was injected into male nu/nu mice bearing subcutaneous HPAC xenografts to estimate rodent dosimetry. SPECT/CT studies showed that the radiotracer accumulates in tumors from 4 – 96 hours post injection, with minimal uptake in normal mouse tissues as expected (Figure 4A). Some increasing radiotracer uptake was observed in the bone, which we propose to be non-specific, as CDCP1 is not abundantly expressed in bone or hematopoietic cells and the bone signal from ^{89}Zr-4A06 was not blocked with excess 4A06. The pattern of biodistribution was qualitatively similar to ^{89}Zr-4A06, as expected. Biodistribution studies were conducted at 0.5, 4, 24, 48, and 96 hours post injection and corroborated the trends suggested by the SPECT imaging data (n = 5/time point, see Figure 4B **and** Supplemental Figure 5).

We next conducted an antitumor assessment study with ^{177}Lu-4A06. The objective of the first study was (1) to test whether a single dose of ^{177}Lu-4A06 can inhibit tumor growth, and (2) to determine if unlabeled 4A06 has measurable effects on tumor burden. To these ends, separate treatment arms of male nu/nu mice bearing subcutaneous HPAC tumors received (1) vehicle, (2) a single intravenous dose of ^{177}Lu-4A06 (800 μCi/mouse), or (3) a single intravenous dose of 50 μg of unlabeled 4A06, comparable to the radiolabeled dose (n = 8/ treatment arm). Over 21 days, ^{177}Lu-4A06 significantly inhibited HPAC tumor growth compared to mice receiving vehicle ($P<0.01$, Figure 5A). Unlabeled 4A06 had no significant effect on tumor growth compared to vehicle.

We next tested if fractionating the dose of ^{177}Lu-4A06 influenced tumor response. A separate cohort of male nu/nu mice bearing HPAC xenografts received (1) vehicle, (2) two intravenous doses of ^{177}Lu-4A06 at day 0 and day 7 of the study (250 μCi/dose), (3) or one intravenous dose of ^{177}Lu-4A06 at day 0 (500 μCi, n = 8/treatment arm). Following tumor responses over 46 days showed that the fractionated dose was more effective at suppressing tumor volume compared to a single dose totaling the same amount of administered radioactivity ($P<0.01$, Figure 5B). Interestingly, although only dose fractionation had a measurable impact on tumor burden at day 46, both treatments extended survival compared to mice receiving vehicle ($P<0.05$, Figure 5C). Both dosing strategies were also equally well tolerated, as no mice were curated from the study due to weight loss >20% (Figure 5D).

Alpha particle emitting radioisotopes have displayed antitumor activity in animal models and humans and may have advantages over β- emitting isotopes for therapies that are delivered within cancer cells (24). After confirming that the 4A06/CDCP1 complex internalizes into cancer cells (Supplemental Figure 6), we next conducted an exploratory

study evaluating the antitumor effects of ^{225}Ac-4A06. The radiopharmaceutical was prepared to >90% radiochemical yield and >99% purity with a specific activity of 0.71 μCi/μg (molar activity = 0.106 Ci/μmol). Intact male nu/nu mice bearing HPAC tumors received a single intravenous injection of ^{225}Ac-4A06 (0.8 μCi) or vehicle (n = 8/arm). ^{225}Ac-4A06 significantly inhibited tumor growth compared to mice receiving vehicle (Figure 5E). Moreover, ^{225}Ac-4A06 treatment significantly lengthened the survival of mice ($P < 0.05$, see Figure 5F). The median survival time of mice in the vehicle group was 15 days, while the median survival of the treated group was 22 days. Mice receiving the ^{225}Ac-4A06 treatment did not experience any unsafe body weight loss (Figure 5G).

Discussion:

In this report, we establish proof of concept that CDCP1 can be targeted for cancer theranostics. An ^{89}Zr-labeled IgG1 platform (clone name 4A06) effectively detected a tumor autonomous antigen expression in numerous human pancreatic cancer cell lines, including two PDX's we established from subjects at UCSF. Although 4A06 alone did not harbor antitumor activity, ^{177}Lu-4A06 effectively inhibited pancreatic cancer growth, particularly when administered as a fractionated dose. Moreover, ^{177}Lu-4A06 was well tolerated in mice and extended overall survival compared to mice that received placebo. An exploratory study showed that ^{225}Ac-4A06 also inhibited pancreatic cancer tumor growth, although the effects did not appear to be as profound as ^{177}Lu-4A06. In summary, these data support further studies to fully vet CDCP1 as a target for cancer theranostics.

We expect it may be possible to even further augment the already impressive antitumor effects we observe with radiolabeled 4A06 IgG1. For instance, there is growing body of data suggesting that cleaved CDCP1 has unique pathologic functions in cancer, including activating prominent signaling cascades and promoting migration and metastasis (18, 25). As full length CDCP1 appears to be the predominant form in normal tissues, antibodies specific to cleaved CDCP1 may increase the tumor specific delivery of cytotoxic payloads(26). As we show, the 4A06 clone itself also does not harbor bioactivity. Thus, developing a radiolabeled form of a bioactive antibody, for example, one that disrupts the initiation of signaling cascades by CDCP1, could further enhance antitumor effects.

Reducing the size of the antibody platform will likely be preferable for more advanced studies in animals or humans. As our autoradiography data show, ^{89}Zr-4A06 IgG1 does not deeply penetrate tumors, and a smaller antibody construct will likely disperse more evenly through tumors based on previous observations in the field (27). This concern is especially germane for pancreatic cancer, which typically induces a desmoplastic reaction. The resulting dense stroma can be challenging for therapeutics to penetrate, which could be a concern for biologic based therapeutics. Although we are cautious to overly speculate, the dense stroma may account for the somewhat milder antitumor effects that we observed with ^{225}Ac-4A06, as its well understood that alpha emitting radioisotopes require close proximity or internalization within the target cell to impart cell death. Radioimmunotherapy with β-emitters, may be less influenced by dense tumor stroma, as crossfire radiation can treat regions of the tumor unbound by drug. Indeed, radioimmunotherapy research has been vibrant with the recent reemergence of nuclear theranostics, and over 15 preclinical trials

testing discrete therapies against targets like CA19.9, MUC1, and integrin α6β4 have shown considerable promise in reducing tumor burden and/or extending overall survival(28). More rigorous comparisons between 4A06 and other experimental therapeutics are warranted to assess the relative strengths and weaknesses of each drug target. Lastly, major sources of grade 3/4 toxicity for radioligand therapies in humans have been hematologic in nature (e.g. thrombocytopenia, neutropenia, anemia) which may be attributable in part to circulating radioactivity. We are currently working to study the impact of antibody size on antitumor efficacy with these observations in mind.

Beyond the considerations mentioned in the introduction, a theranostic strategy is particularly attractive for a tumor antigen like CDCP1 as the imaging can be used to prospectively identify patients whose tumors have high levels of expression. At a population level, near complete (~90%) antigen overexpression has only been noted to date in the clear cell form of ovarian cancer, and expression in more common cancers (including PDAC) is typically between 30 – 60%. Moreover, imaging may provide a more holistic view of antigen expression over many tumor sites within the same patient to reveal whether CDCP1 expression is heterogeneous.

Supplementary Material

Refer to Web version on PubMed Central for supplementary material.

Acknowledgments:

We gratefully acknowledge Dr. Henry VanBrocklin, Dr. Denis Beckford-Vera, and Joseph Blecha for assistance with radiochemistry and Tony Huynh for assistance with small animal PET/CT studies. Small animal PET/CT and SPECT/CT studies were performed on instruments supported by National Institutes of Health grants S10RR023051 and S10OD012301. E.A.C. received funding from the National Cancer Institute (U24CA210974, R01CA222862, R01CA227807, R01CA239604, R01CA230263). Patient tumor xenografts were constructed and studied with support from the V Foundation (Translational Grant A130433, PI: K.S.K). J.A.W. acknowledges funding from NCI 1P41CA196276, CA191018, NIH GM097316; and Celgene Corp. S.L. was supported by Helen Hay Whitney post-doctoral fellowship. J.Z. was supported by an NIH post-doctoral fellowship. M. J. Evans acknowledges funding from the American Cancer Society (Research Scholar Grant 130635-RSG-17-005-01-CCE), the Precision Imaging of Cancer and Therapy program at UCSF, and the National Institutes of Health (R01MH114053, R01EB025027).

References:

1. Jadvar H, Chen X, Cai W, Mahmood U. Radiotheranostics in Cancer Diagnosis and Management. Radiology. 2018;286:388–400. [PubMed: 29356634]
2. Hooper JD, Zijlstra A, Aimes RT, Liang H, Claassen GF, Tarin D, et al. Subtractive immunization using highly metastatic human tumor cells identifies SIMA135/CDCP1, a 135 kDa cell surface phosphorylated glycoprotein antigen. Oncogene. 2003;22:1783–94. [PubMed: 12660814]
3. Wortmann A, He Y, Deryugina EI, Quigley JP, Hooper JD. The cell surface glycoprotein CDCP1 in cancer--insights, opportunities, and challenges. IUBMB life. 2009;61:723–30. [PubMed: 19514048]
4. Chou CT, Li YJ, Chang CC, Yang CN, Li PS, Jeng YM, et al. Prognostic Significance of CDCP1 Expression in Colorectal Cancer and Effect of Its Inhibition on Invasion and Migration. Annals of surgical oncology. 2015;22:4335–43. [PubMed: 25820997]
5. Turdo F, Bianchi F, Gasparini P, Sandri M, Sasso M, De Cecco L, et al. CDCP1 is a novel marker of the most aggressive human triple-negative breast cancers. Oncotarget. 2016;7:69649–65. [PubMed: 27626701]

6. He Y, Wu AC, Harrington BS, Davies CM, Wallace SJ, Adams MN, et al. Elevated CDCP1 predicts poor patient outcome and mediates ovarian clear cell carcinoma by promoting tumor spheroid formation, cell migration and chemoresistance. Oncogene. 2016;35:468–78. [PubMed: 25893298]
7. Ikeda J, Oda T, Inoue M, Uekita T, Sakai R, Okumura M, et al. Expression of CUB domain containing protein (CDCP1) is correlated with prognosis and survival of patients with adenocarcinoma of lung. Cancer science. 2009;100:429–33. [PubMed: 19077003]
8. Awakura Y, Nakamura E, Takahashi T, Kotani H, Mikami Y, Kadowaki T, et al. Microarray-based identification of CUB-domain containing protein 1 as a potential prognostic marker in conventional renal cell carcinoma. Journal of cancer research and clinical oncology. 2008;134:1363–9. [PubMed: 18483744]
9. Emerling BM, Benes CH, Poulogiannis G, Bell EL, Courtney K, Liu H, et al. Identification of CDCP1 as a hypoxia-inducible factor 2alpha (HIF-2alpha) target gene that is associated with survival in clear cell renal cell carcinoma patients. Proc Natl Acad Sci U S A. 2013;110:3483–8. [PubMed: 23378636]
10. Miyazawa Y, Uekita T, Hiraoka N, Fujii S, Kosuge T, Kanai Y, et al. CUB domain-containing protein 1, a prognostic factor for human pancreatic cancers, promotes cell migration and extracellular matrix degradation. Cancer Res. 2010;70:5136–46. [PubMed: 20501830]
11. Martinko AJ, Truillet C, Julien O, Diaz JE, Horlbeck MA, Whiteley G, et al. Targeting RAS-driven human cancer cells with antibodies to upregulated and essential cell-surface proteins. Elife. 2018;7.
12. Uekita T, Fujii S, Miyazawa Y, Iwakawa R, Narisawa-Saito M, Nakashima K, et al. Oncogenic Ras/ERK signaling activates CDCP1 to promote tumor invasion and metastasis. Molecular cancer research : MCR. 2014;12:1449–59. [PubMed: 24939643]
13. Noskovicova N, Heinzelmann K, Burgstaller G, Behr J, Eickelberg O. Cub domain-containing protein 1 negatively regulates TGF-beta signaling and myofibroblast differentiation. American journal of physiology Lung cellular and molecular physiology. 2018;314:L695–L707. [PubMed: 29351434]
14. Spassov DS, Wong CH, Wong SY, Reiter JF, Moasser MM. Trask loss enhances tumorigenic growth by liberating integrin signaling and growth factor receptor cross-talk in unanchored cells. Cancer research. 2013;73:1168–79. [PubMed: 23243018]
15. Uekita T, Sakai R. Roles of CUB domain-containing protein 1 signaling in cancer invasion and metastasis. Cancer science. 2011;102:1943–8. [PubMed: 21812858]
16. Wright HJ, Hou J, Xu B, Cortez M, Potma EO, Tromberg BJ, et al. CDCP1 drives triple-negative breast cancer metastasis through reduction of lipid-droplet abundance and stimulation of fatty acid oxidation. Proceedings of the National Academy of Sciences of the United States of America. 2017;114:E6556–E65. [PubMed: 28739932]
17. He Y, Harrington BS, Hooper JD. New crossroads for potential therapeutic intervention in cancer - intersections between CDCP1, EGFR family members and downstream signaling pathways. Oncoscience. 2016;3:5–8. [PubMed: 26973855]
18. Casar B, Rimann I, Kato H, Shattil SJ, Quigley JP, Deryugina EI. In vivo cleaved CDCP1 promotes early tumor dissemination via complexing with activated beta1 integrin and induction of FAK/PI3K/Akt motility signaling. Oncogene. 2014;33:255–68. [PubMed: 23208492]
19. Orchard-Webb DJ, Lee TC, Cook GP, Blair GE. CUB domain containing protein 1 (CDCP1) modulates adhesion and motility in colon cancer cells. BMC cancer. 2014;14:754. [PubMed: 25301083]
20. Harrington BS, He Y, Davies CM, Wallace SJ, Adams MN, Beaven EA, et al. Cell line and patient-derived xenograft models reveal elevated CDCP1 as a target in high-grade serous ovarian cancer. British journal of cancer. 2016;114:417–26. [PubMed: 26882065]
21. Miura S, Hamada S, Masamune A, Satoh K, Shimosegawa T. CUB-domain containing protein 1 represses the epithelial phenotype of pancreatic cancer cells. Experimental cell research. 2014;321:209–18. [PubMed: 24384474]
22. Zeglis BM, Houghton JL, Evans MJ, Viola-Villegas N, Lewis JS. Underscoring the influence of inorganic chemistry on nuclear imaging with radiometals. Inorganic chemistry. 2014;53:1880–99. [PubMed: 24313747]

23. Holland JP, Sheh Y, Lewis JS. Standardized methods for the production of high specific-activity zirconium-89. Nuclear medicine and biology. 2009;36:729–39. [PubMed: 19720285]

24. Targeted Alpha Therapy Working G, Parker C, Lewington V, Shore N, Kratochwil C, Levy M, et al. Targeted Alpha Therapy, an Emerging Class of Cancer Agents: A Review. JAMA oncology. 2018;4:1765–72. [PubMed: 30326033]

25. Wright HJ, Arulmoli J, Motazedi M, Nelson LJ, Heinemann FS, Flanagan LA, et al. CDCP1 cleavage is necessary for homodimerization-induced migration of triple-negative breast cancer. Oncogene. 2016;35:4762–72. [PubMed: 26876198]

26. He Y, Wortmann A, Burke LJ, Reid JC, Adams MN, Abdul-Jabbar I, et al. Proteolysis-induced N-terminal ectodomain shedding of the integral membrane glycoprotein CUB domain-containing protein 1 (CDCP1) is accompanied by tyrosine phosphorylation of its C-terminal domain and recruitment of Src and PKCdelta. The Journal of biological chemistry. 2010;285:26162–73. [PubMed: 20551327]

27. Wittrup KD, Thurber GM, Schmidt MM, Rhoden JJ. Practical theoretic guidance for the design of tumor-targeting agents. Methods in enzymology. 2012;503:255–68. [PubMed: 22230572]

28. Hull A, Li Y, Bartholomeusz D, Hsieh W, Allen B, Bezak E. Radioimmunotherapy of Pancreatic Ductal Adenocarcinoma: A Review of the Current Status of Literature. Cancers (Basel). 2020;12.

Statement of translational relevance:

CDCP1 is highly overexpressed in many deadly cancer types, including pancreatic, triple negative breast cancer, lung, and prostate cancer. However, CDCP1 has not been tested clinically and is relatively unexplored as a drug target. The results from this study show that CDCP1 can be targeted therapeutically using a clinically validated strategy, namely the focal ablation of tumor cells with ionizing radiation from a systemically administered radioligand. These data provide the scientific rationale for further studies to identify the optimal ligand platform and radioisotope to fully exploit the restricted overexpression of CDCP1 in cancer.

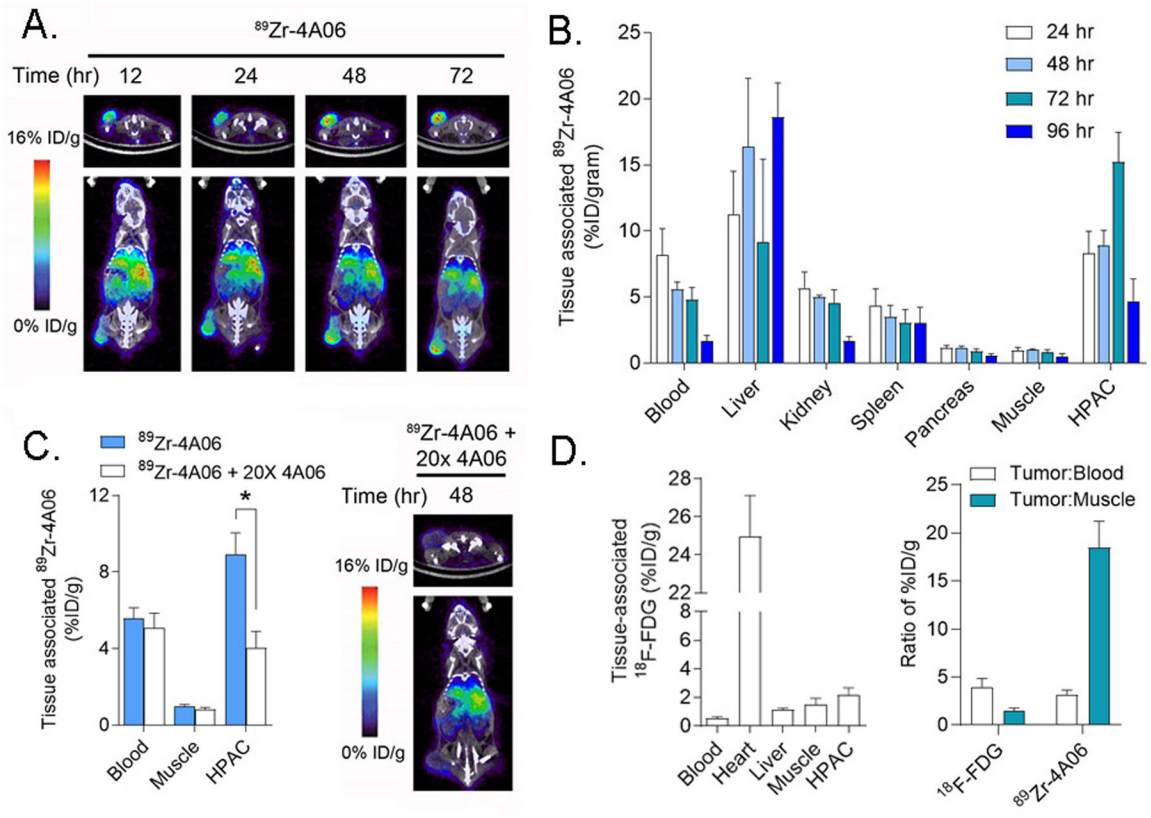

Figure 1. Detection of tumor autonomous expression of CDCP1 in a human pancreatic cancer model with ^{89}Zr-4A06 PET/CT.

A. Representative transverse and coronal PET/CT images of a mouse bearing a subcutaneous HPAC xenograft at various time points after administration of ^{89}Zr-4A06. The tumor is visible on the left hindlimb of the mouse. Some radiotracer accumulation is observed in normal abdominal tissues associated with immunoglobulin clearance, as expected. **B.** Ex vivo biodistribution data showing the accumulation of ^{89}Zr-4A06 in mice bearing HPAC tumors over time. Tumor uptake of the radiotracer peaks at 72 hours post injection, while normal tissue accumulation is generally lower (n = 4/time point). **C.** At left are shown biodistribution data collected 48 hours post injection of ^{89}Zr-4A06 or ^{89}Zr-4A06 coadministered with 20x molar excess unlabeled 4A06 (n = 4/arm, *P<0.01). The excess antibody suppresses radiotracer binding in the tumor, as expected. At right are shown transverse and coronal PET/CT images of one mouse from the treatment arm that received ^{89}Zr-4A06 with 20x unlabeled 4A06. **D.** At left are shown biodistribution data highlighting the uptake of ^{18}F-fluorodeoxyglucose 60 minutes post injection in mice bearing subcutaneous HPAC tumors (n = 4). The level of uptake is lower than what was observed for ^{89}Zr-4A06. Selected normal tissues are shown for comparison. At right are shown a comparison of the tumor to blood and tumor to muscle ratios for ^{18}F-FDG (60 min post injection) and ^{89}Zr-4A06 (72 hours post injection).

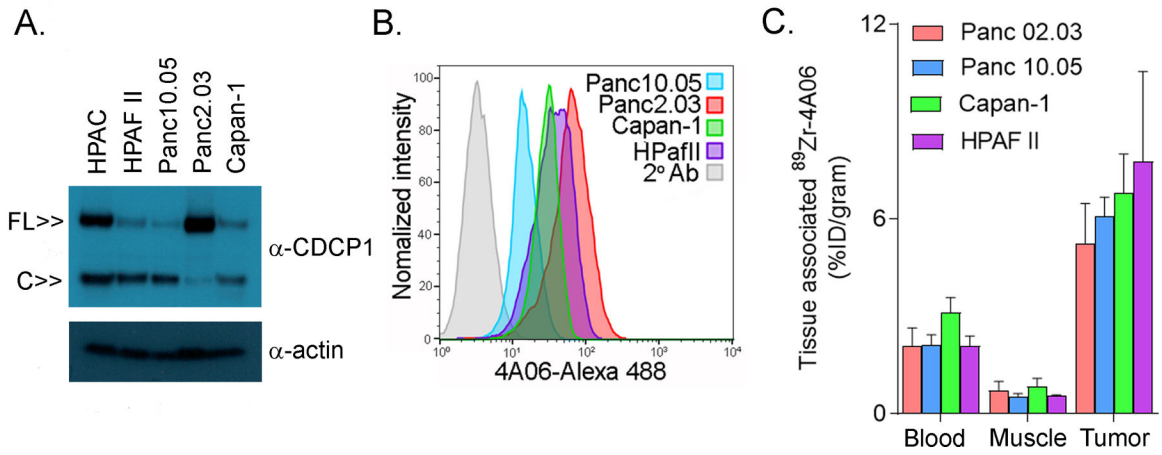

Figure 2. ^{89}Zr-4A06 PET/CT detects pancreatic cancer models with diverse presentations of full length and/or cleaved CDCP1.

A. Immunoblot data from whole cell lysates showing the relative expression of full length (~140 kDa) and cleaved (~80 kDa) CDCP1 in four human PDAC cell lines. HPAC is included as a reference. **B.** Histograms showing the binding of 4A06-Alexa488 to cell surface CDCP1 on pancreatic cancer cell lines. **C.** Biodistribution showing the uptake of ^{89}Zr-4A06 in subcutaneous tumors in mice (n = 4/tumor). The data were collected 72 hours post injection. Radiotracer levels in blood and muscle are shown as references. The level of radiotracer uptake in HPAC tumors at 72 hours post injection was statistically higher than Capan-1, Panc02.03, and Panc10.05 (Supplemental Table 2).

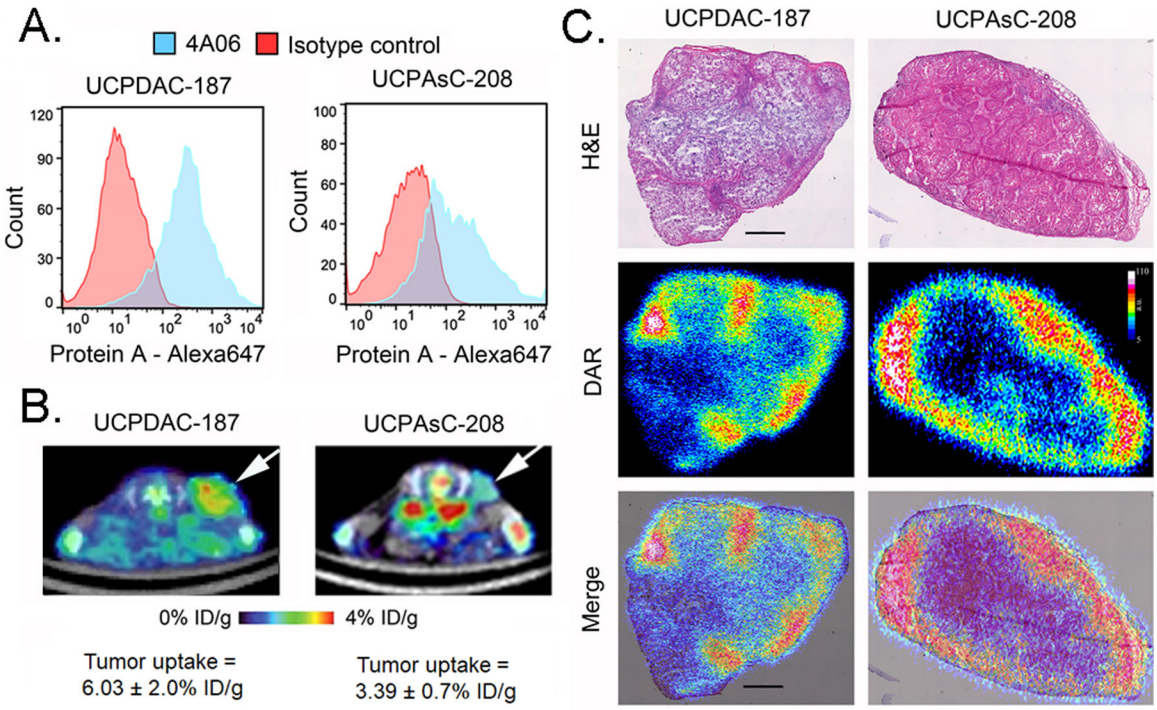

Figure 3. CDCP1 is expressed and detectable with ^{89}Zr-4A06 PET/CT in two PDX models of pancreatic cancer.

A. Histograms from single cell suspensions of two PDX models, UCPDAC-187 and UCAsC-208, show positive staining for CDCP1 using 4A06 and a secondary anti-protein A antibody coupled to Alexa647. The data are referenced against background staining with a commercial IgG1 isotype control. **C.** Transverse PET/CT images showing the uptake of ^{89}Zr-4A06 in the subcutaneous PDX tumors (white arrows). The data were acquired 48 hours post injection of the radiotracer, and the position of the tumor is indicated with an arrow. The tumor uptake of ^{89}Zr-4A06 at 48 hours post injection is indicated below the respective image (n = 4/tumor). **D.** Digital autoradiography (DAR) of PDX tissue slices show the distribution of ^{89}Zr-4A06 within the tumor. The radioactivity is primarily localized to periphery of the tumor, whose morphology is defined with H&E. The scale bar represents 100 μm.

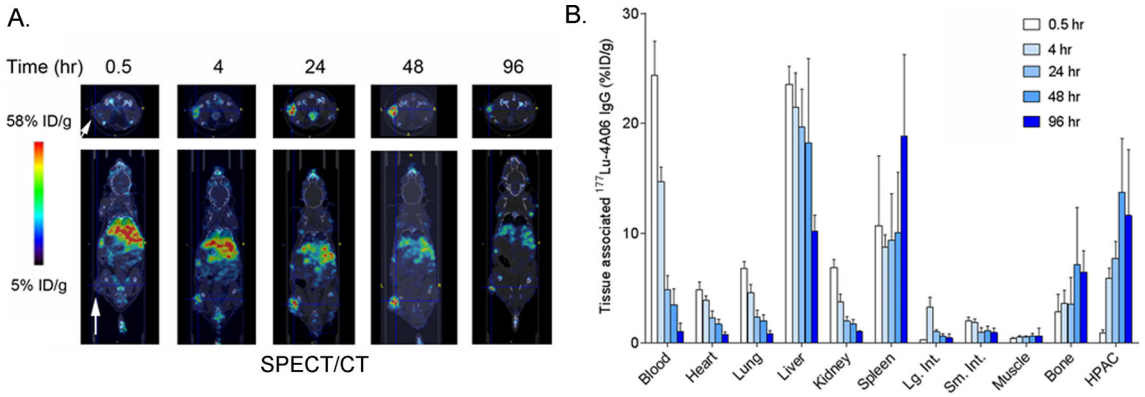

Figure 4. SPECT/CT and biodistribution data shows the accumulation of ^{177}Lu-4A06 IgG1 in HPAC tumors and normal mouse tissues.

A. Representative transverse and coronal SPECT/CT data showing tumor uptake in subcutaneous HPAC tumors (white arrow) over time. As with ^{89}Zr-4A06, the radiotracer uptake in tumors peaks after 48 hours post injection. Nonspecific uptake is observed in abdominal tissues, as expected based on the data with ^{89}Zr-4A06. **B.** Ex vivo biodistribution data showing the accumulation of ^{177}Lu-4A06 in tissues over time (n = 4/time point). The biodistribution is qualitatively similar to what was observed with ^{89}Zr-4A06.

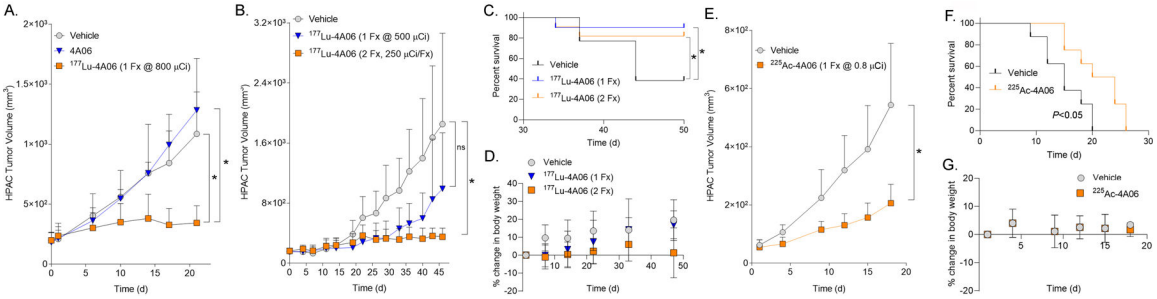

Figure 5. ^{177}Lu-4A06 and ^{225}Ac-4A06 inhibit tumor growth in animal models of pancreatic cancer.

A. An antitumor assessment study in which mice bearing subcutaneous HPAC tumors received a single bolus of ^{177}Lu-4A06 (800 µCi/mouse), vehicle, or unlabeled 4A06. ^{177}Lu-4A06 significantly suppressed tumor growth compared vehicle or 4A06 alone (n = 8/treatment arm, *P<0.01) **B.** Tumor growth curves summarizing the antitumor effects of a single bolus of ^{177}Lu-4A06 (500 µCi) or two doses of ^{177}Lu-4A06 (250 µCi/dose) over seven days. Mice bearing subcutaneous HPAC tumors were treated. Only the fractionated dose significantly inhibited tumor growth compared to the vehicle treatment arm (n = 8/treatment arm). **C.** A Kaplan Meier curve showing that either dosing regimen extended survival compared to mice receiving vehicle. Statistical significance was determined using a Mantel-Cox log rank test. *P <0.05. **D.** A plot showing the percent change in body weight for mice receiving vehicle or ^{177}Lu-4A06. Neither dosing strategy resulted in dropout due to >20% loss of body weight. **E.** A tumor growth curve summarizing the effects of ^{225}Ac-4A06 on the growth of subcutaneous HPAC tumors. A single intravenous injection of ^{225}Ac-4A06 (0.8 µ**Ci**/mouse) significantly delayed tumor growth compared to mice receiving vehicle (n = 8/treatment arm). **F.** A Kaplan Meier curve showing that ^{225}Ac-4A06 extended survival compared to mice receiving vehicle. Statistical significance was determined using a Mantel-Cox log rank test. ***P < 0.05. The median survival of the vehicle group was 15 days, while the median survival of the treated group was 22 days. The log rank hazard ratio was 2.56 (95% CI = 0.8 – 7.6). **G.** A plot showing the average percent change in body weight for mice receiving vehicle or ^{225}Ac-4A06. No mice dropped from the study due to an unsafe loss of body weight.